Contents lists available at http://qu.edu.iq

Al-Qadisiyah Journal for Engineering Sciences

Journal homepage: https://qjes.qu.edu.iq

Effects of fin on mixed convection heat transfer in a vented square cavity: A numerical study

Mohammed Abu Ghurban [a], ***Khaled Al-Farhany*** [a]*, ***and Kada Benhanifia*** [b]

[a]*Department of Mechanical Engineering, University of Al-Qadisiyah, Al-Diwaniyah, 58001, Iraq*

[b]*Laboratory of Energy in Arid Region (ENERGARID), Faculty of Science and Technology, University of Tahri Mohamed Bechar, P.O. Box 417, Bechar 08000, Algeria*

A R T I C L E I N F O

Article history:
Received 30 January 2023
Received in revised form 27 July 2023
Accepted 28 August 2023

Keywords:
Mixed convection
Heat transfer
Laminar flow
Open cavity
Fin

A B S T R A C T

Numerical investigation of mixed convective in a vented square cavity with fin. The horizontal walls are adiabatic, while the left and right walls are hot (T_h) and cold (T_c) temperatures, respectively. The fluid inlet to the cavity from the lower left open area(W_{in}), and exits from the upper right open area (W_{out}). In this study, a finite element scheme is employed. The analysis is done for specific Prandtl number ($Pr = 7$), Reynolds number ($50 \leq Re \leq 200$), fin length $(0.2 \leq L_f \leq 0.6)$, Richardson number ($0.1 \leq Ri \leq 1$), and the location of the fin ($0.2 \leq h \leq 0.6$). The finding indicates that the Nu_{avg} increases when high the location of the fin increases at the maximum height of this fin location is estimated to be 17% due to an increase in the fluid flow area on the hot wall caused by rising convective. The highest heat transfer occurs when the fin length equals 0.6 at the location($h = 0.2$).

1. Introduction

The subject of convective heat transfer and fluid flow within enclosure areas has always drawn academics because of how prevalent it is. Convective heat transport is frequently split into three categories: forced convection ($Ri < 0.1$), natural convection ($Ri > 10$), and mixed convection ($0.1 \leq Ri \leq 10$). Convective heat transport has several applications, including heat exchangers[1], solar collectors [2], electronics equipment cooling [3, 4], etc. AL-Farhany et al.[5, 6] examined the impact of the inclined baffle on free convective in a container filled with different nanofluid (Al_2O_3-water) and (Cu-water). The left side was thick and hot, while the right side was cold, and the other were adiabatic. The outcome is reduced heat transfer when increasing the thickness of the hot wall. When the angle of the baffle was equal to 60, the stream function was at its maximum. As well as examine the impact of sinusoidal temperature AL-Farhany et al. [7]. Al-Maliki et al. [8] studied experimental free convective in a rectangular container filled with a hybrid nanofluid. PCM was attached to a heated wall; the opposite wall was cold, while the other parts were adiabatic. The result was that the PCM was also discovered to have the potential to lower the temperature of the hot wall by as much as 22%. Al-Farhany et al.[9, 10] studied the examination effect of MHD in a porous enclosure with two fins. Selimefendigil and Oztop [11] study the numerical impact of the baffle on mixed convective in a vented cavity. The horizontal walls were hot, while the vertical walls were adiabatic. The inclined baffle is fixed on half the lower wall. The upper limit of the Nusselt number was achieved at angles ($\emptyset = 30, 90$).

* *Corresponding author.*
E-mail address: khaled.alfarhany@qu.edu.iq (Khaled Al-Farhany)

https://doi.org/10.30772/qjes.2023.142305.1016

Nomenclature:

g	gravitational acceleration	*Greek symbols*	
h	fin locations	β	thermal expansion coefficient
K_r	thermal conductivity ratio, $K_r = K_s/K_f$	θ	dimensionless temperature
L	length of the cavity	ν	kinematic viscosity
L_f	length of the fin	α	thermal diffusivity
Nu	local Nusselt number	μ	dynamic viscosity
Nu_{avg}	average Nusselt number	Ψ	streamlines
p	pressure	σ	stress tensor
P	non-dimensional pressure	ρ	density
Pr	Prandtl number		
Re	Reynolds number	*Subscripts*	
Ri	Richardson number	c	cold temperature
T	dimensional temperature	h	hot temperature
U, V	dimensionless velocity components	f	fluid
W	sizes of inlet and outlet holes	s	solid
X, Y	dimensionless coordinates	r	ratio

Sivasankaran and Janagi [12] analyzed mixed convective in an oblique channel under the impact of the baffle. Its focus on baffle length (L_b), inclined angle ($\emptyset$), and Richardson number (Ri). It found that when the baffle length is greater, heat transference increases. Velkennendy et al. [13, 14] studied mixed convective in a rectangular open enclosure. The fins are attached to the upper wall. The lower wall was adiabatic, while the others were hot temperature. Air was utilized as a working fluid. The result demonstrated the rise in buoyancy force enhances heat transport. Abdulsahib and Al-Farhany [15] experimentally studied mixed convective on a rotating cylinder in a porous nanofluid enclosure. The upper half was filled with (Al_2O_3-water), the lower half was porous media, and a rotating cylinder was situated in a central location. The vertical walls were at various temperatures, while the horizontal walls were adiabatic. The finding revealed that the upper part of the cavity had excellent temperature distribution, while the lower part was temperature only near the hot side. Additionally, the impact of MHD in three-dimensional (3D) open enclosures was studied by Selimenfendigil and Chamkha [16]. Mixed convective in a square chamber with several ventilation ports was studied by Alhussain [17]. Shaker et al. [18] examined the impact of a magnetic field on mixed convective in a vented cavity. The influence of altering factors Reynold's number ($200 \le Re \le 600$), and magnetic number ($0 \le Mn \le 5 \times 10^7$). The magnetic field's i'fluence on heat and flow properties was less pronounced at the high Reynold number. Wang et al. [19] studied the influence of lid-driven in rectangular on mixed convective. Ali et al. [20] add to the work the effect of a magnetic field and cylinder in the center. The heat transfer rises by increasing the speeds of the cylinder, and reduce by increasing Hartmann number. Recently, many researches had been made for mixed convection with fins/ baffle in different an open cavity or channels [21-25].

As seen from the above review, there is no research in the literature on the impact of single fin lengths and fin locations for mixed convective in a vented cavity system. This issue has numerous uses in cooling both thermal systems and electronic equipment. Consequently, the current study examines the impact of fin lengths (L_f), fin locations (h), Richardson number (Ri), and Reynolds numbers (Re) on mixed convective in a vented cavity.

2. Physical model description

The two dimension (2D) square vented cavity is demonstrated in **Fig. 1**. The horizontal side walls are adiabatic, while the left and right walls are hot (T_h), and cold (T_c) temperature, respectively. The single fin is fixed to the hot vertical wall at various lengths ($L_f = 0.2, 0.4, and\ 0.6$), and various location ($h = 0.2, 0.4, and\ 0.6$), while the fin thickness is assumed to be fixed and equal to ($t_f = 0.02L$). The thermal conductivity of aluminum fin is equal to 239. The cold fluid inlet to the enclosure from the lower side at the open area is equal to ($W_{in} = 0.1$), and left the cavity from the outlet area on the right upper side ($W_{out} = 0.1$). The fluid inlet at cold temperature (T_c), while it is assumed to leave the cavity at atmospheric pressure. Water has been chosen as the working fluid at Prandtl number equal to ($Pr = 7$).

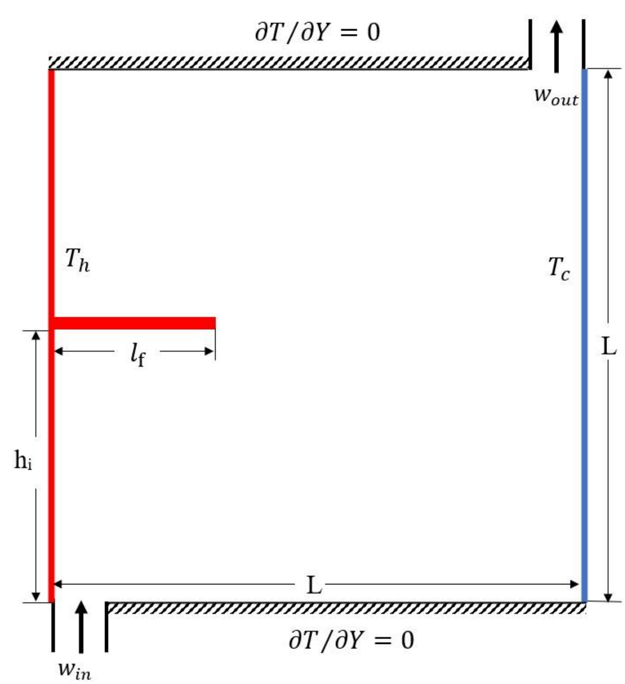

Figure 1. Diagram of the model

2.1. The equations of the conservation

The governing equations in the current work for continuity, momentum, and energy are provided in their dimensionless form are [11, 12]:

$$\frac{\partial U}{\partial X} + \frac{\partial V}{\partial Y} = 0 \quad (1)$$

$$U\frac{\partial U}{\partial X} + V\frac{\partial U}{\partial Y} = -\frac{\partial P}{\partial X} + \frac{1}{Re}\left(\frac{\partial^2 U}{\partial X^2} + \frac{\partial^2 U}{\partial Y^2}\right) \quad (2)$$

$$U\frac{\partial V}{\partial X} + V\frac{\partial V}{\partial Y} = -\frac{\partial P}{\partial Y} + \frac{1}{Re}\left(\frac{\partial^2 V}{\partial X^2} + \frac{\partial^2 V}{\partial Y^2}\right) + Ri\,\theta \quad (3)$$

$$U\frac{\partial\theta}{\partial X}+V\frac{\partial\theta}{\partial Y}=\frac{1}{Re\,Pr}\left(\frac{\partial^2\theta}{\partial X^2}+\frac{\partial^2\theta}{\partial Y^2}\right) \quad (4)$$

The energy equation of the fins: [5-7]

$$\frac{\partial^2\theta}{\partial X^2}+\frac{\partial^2\theta}{\partial Y^2}=0 \quad (5)$$

The non-dimensional parameters in the above equations used are:

$$X=\frac{x}{L},Y=\frac{y}{L},L_f=\frac{l_f}{L},W=\frac{w}{L},h=\frac{hi}{L},\ U=\frac{u}{U_\circ},V=\frac{v}{U_\circ},P=\frac{p}{\rho U_\circ^2},\theta=\frac{T-T_c}{T_h-T_c},Pr=\frac{\nu}{\alpha} \quad (6)$$

Three dimensionless factors can be used to determine mixed convection: the Grashof number (Gr), Reynolds number (Re), and Richardson number (Ri) expressed as:

$$Gr=\frac{g\beta(T_h-T_c)L^3}{\upsilon^2},Re=\frac{\rho U_\circ L}{\mu},Ri=\frac{Gr}{Re^2} \quad (7)$$

2.2. Boundary conditions

Non-dimensional boundary conditions are given in Table 1. As shown below.

Table 1. Dimensionless boundary conditions

Location	Boundary conditions
The left wall	$U=V=0,\theta=1,\ X=0,\ 0\le Y\le 1$
The right wall	$U=V=0,\theta=0\ ,\ X=1,0\le Y\le 1$
The bottom wall	$U=V=0,\partial\theta/\partial y=0,\ W_{in}\le X\le 1,Y=0$
The upper wall	$U=V=0,\partial\theta/\partial y=0,\ 0\le X\le 1-W_{out},Y=1$
At the inlet	$U=0,V=1,\ \theta=0,0\le X\le W_{in},Y=0$
At the outlet	$P=0,(1-W_{out})\le X\le 1,\ Y=1$
The fin	$U=V=0,\ (\partial\theta/\partial n)_f=K_r(\partial\theta/\partial n)_s$

2.3. Local Nusselt number

The Nusselt number applies to express the characteristics of the heat transfer rate [5-7]:

The local Nusselt number of the said left wall.

$$Nu=-\left.\frac{\partial\theta}{\partial x}\right|_{x=0} \quad (8)$$

The average Nusselt number of the said left wall.

$$Nu_{avg}=\int_0^1 Nu\,dy \quad (9)$$

3. Numerical solutions

COMSOL Multiphysics system version (6) has been used to implement the finite element technique in the current simulation. This system is significant as a strong alternate strategy for several models that consider variable resolution and allow the usage of unstructured grids. This approach solves the Navier stock and energy equations, and the model's analysis is shown. Triangular elements are employed in the mesh generation. **Fig. 2** depicts a two-dimensional (2D) domain in a Cartesian coordinate divided into many parts as triangular meshes. All of the variables (*P*, *U*, *V*, and *C*) are taken into consideration when the convergence of the following occurs:

$$\left|\frac{\xi^{i+1}-\xi^i}{\xi^{i+1}}\right|\le 10^{-5} \quad (10)$$

Table 2 demonstrates how the average Nusselt number on the hot wall is impacted by mesh size for $Pr=7,Re=100,Ri=0.9,L_f=0.4$, and $h=0.4$. The average Nusselt number (Nu_{avg}) of mesh 4 (22642 elements) which varies little from the outcomes obtained from the other mesh sizes, where the error was 1.74%. As a result, mesh 4 produced all the cases.

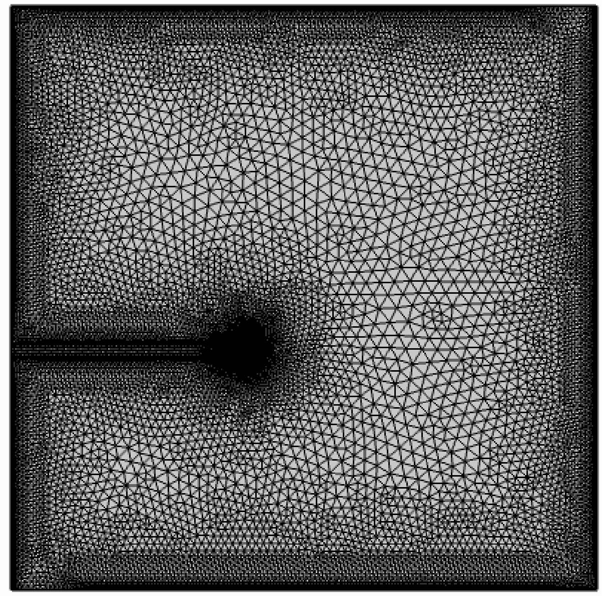

Figure 2. The mesh generation for the cavity

Table 2. Demonstrates the average Nusselt number ($\boldsymbol{Nu_{avg}}$) on the hot wall and the mesh sizes for $\boldsymbol{Pr=7,Re=100,Ri=0.9,L_f=0.4}$, and $\boldsymbol{h=0.4}$.

Sizes of mesh	*Elements of Mesh*	Average Nusselt number
Mesh 1	2191	8.8999
Mesh 2	3440	8.9904
Mesh 3	8735	9.3611
Mesh 4	22642	9.5241
Mesh 5	31244	9.5248

3.1. Validation

To ensure simulation accuracy for a cavity with a fin, **Fig. 3** depicts work validation of isotherms and streamlines. The validation is done with Sathiyamoorthy and Chamkha's [26] work. Examination of free convective in a square shape with fixed fin in half the lower wall at Raynold number ($Ra=10^5$), Prandtl number ($Pr=100$), and the fin length($L_f=0.25$). The output results are accurate and of great quality. The second validation was done with Rahman et al. [27]. Mixed convective in an open enclosure filled with air. **Table 3** illustrates the average Nusselt number on the right wall at $Pr=0.71,Re=100$, and various Richardson number.

Table 3. Average Nusselt number ($\boldsymbol{Nu_{avg}}$) on the hot wall at $\boldsymbol{Pr=0.71,Re=100}$.

	Rahman et al. [27]	Present work
$Ri=1$	4.7	4.62
$Ri=3$	5.35	5.32
$Ri=4$	5.56	5.51
$Ri=5$	5.71	5.65

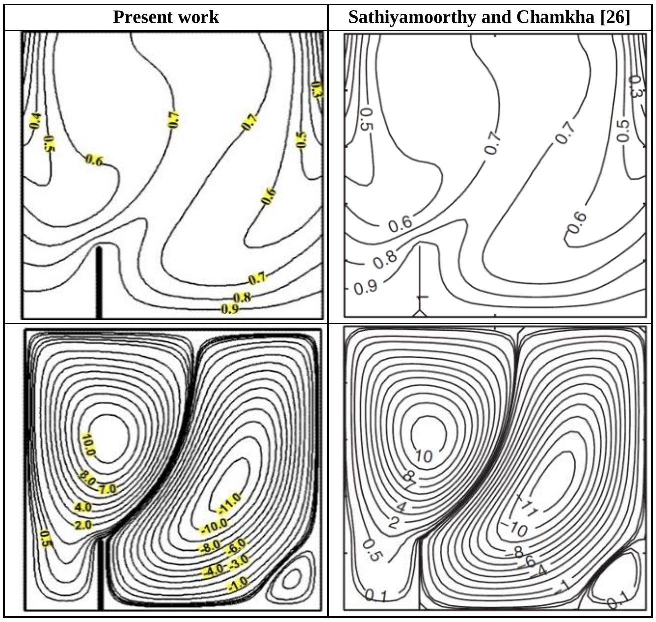

Figure 3. Comparison of isotherms and streamlines of the present results with Sathiyamoorthy and Chamkha [26] at $\boldsymbol{Pr = 100}$, $\boldsymbol{Ra = 10^5}$, and $\boldsymbol{L_f = 0.25}$.

4. Results

Numerical analysis mixed convective is accomplished in a two-dimensional (2D) cavity with a present fin attached to the left hot wall. The cold fluid enters the enclosure through the open area (W_{in}) in the lower left corner and escapes through the open area (W_{out}) in the upper right corner. Water is employed as the working fluid and has been assigned the Prandtl number ($Pr = 7$). The outcomes of this study in this part demonstrate the influence of dimensionless characteristics: Reynold number (Re), Richardson number (Ri), fin lengths (L_f), and fin locations (h). For all of the aforementioned factors, the findings are demonstrated in terms of streamline (Ψ), isothermal (θ), and average Nusselt number (Nu_{avg}). The dimensionless variable ranges are:

1. Reynolds number ($50 \leq Re \leq 200$).
2. Richardson number ($0.1 \leq Ri \leq 1$).
3. Fin lengths ($0.2 \leq L_f \leq 0.6$).
4. Fin locations ($0.2 \leq h \leq 0.6$).

4.1. Effect of Reynolds number with h

Figs. 4, 5. Demonstrate the Reynold number's (Re) impact on the streamlines (Ψ) and isothermal (θ) for various fin locations (h) for $Pr = 7, Ri = 0.1$, and $L_f = 0.4$. When the Reynold number is low, a large vortex forms above the fin, and when it is high, the impact of the inertia force causes the vortex to grow and be stronger. In the second column, for fin location ($h = 0.4$), increase the flow in an enclosure, and vortices form adjacent to the lower wall due to the separation process. In the third column, which fin location was ($h = 0.6$), the flow now occupies most parts of the enclosure because of the high location of the fin, where the flow is from left to right. Due to the increased inertial force, circular vortices in the lowest portion of the container became intensive. **Fig. 5** demonstrates the Reynold number's (Re) impact on isothermal (θ) for various fin locations. The isothermal lines are vertical, when Re is increased, we observe that the cooling process improves due to the increase in the flow of cold fluid. When increasing the height of the fin location (h), it was observed that the heat transport is limited in the area above the fin.

4.2. Effect of Richardson number with h

Figs. 6 and 7, demonstrate the Richardson number's (Ri) impact on the streamlines (Ψ) and isothermal (θ) for various fin locations (h) for $Pr = 7, Re = 100$, and $L_f = 0.4$. In the first column, at a low Richardson number, the flow is high due to the force convective being dominant. When the Richardson number rises, the flow takes the shape of an S, as it expands in all parts of the container. In the second column, there is the presence of a vortex in the upper half, and when Ri rises, it forms a small vortex in the lower. In the third column, which fin location was ($h = 0.6$), very dense swirls in the lower half of the container due to the increased buoyancy force influence. **Fig. 7** demonstrates the Richards number's (Ri) impact on isothermal (θ) for various fin locations. In the first column, for ($h = 0.2$) at the lower Richardson number, the heat transport from the left side to the right side enhances, which is dominated by convective force. When rising Richards number (Ri), the chilly wall's impact is starting to become apparent as the natural convective. When there is a high fin placement lower triangle becomes cold, while the upper triangle becomes hot.

4.3. Effect of fin lengths with h

Figs. 8 and **9**. Demonstrate the fin lengths (L_f) impact on the streamlines (Ψ) and isothermal (θ) for various fin locations (h) for $Pr = 7, Re = 50$, and $Ri = 1$. In the first column, for ($h = 0.2$), the fluid takes up all of the container's space, and the fluid restriction increases as fin length increases. In the second column, the fin location was ($h = 0.4$). The flow is aligned to the walls, while a small vortex is formed in the opposite corner of the inlet hole. In the third column, the fin location was ($h = 0.6$), form big circulation at the lower of the cavity; the flow takes a different shape when increasing the fin length. **Fig. 9** demonstrates the fin lengths (L_f) impact on isothermal (θ) for various fin locations. As the length of the fin rises, the process of heat transport improves due to the fin's high thermal conductivity. At its fin's maximum height, the greatest heat exchange occurs between the fluid and the hot wall.

4.4. Average Nusselt number

Fig. 10. explains the influence of Reynold's number on the average Nusselt number (Nu_{avg}) at hot wall for $Pr = 7, Ri = 0.9$, and $h = 0.2$. Nu_{avg} increases with reduced length of fin (L_f), and rising Reynold number (Re), respectively. When the Reynold number rises from 50 to 200 for fin length ($L_f = 0.6$), the average Nusselt number rises by approximately 50.68 % due influence of inertia forces. **Fig. 11**. explains the influence of Richardson's number on the average Nusselt number (Nu_{avg}) at hot wall for $Pr = 7, Re = 100$, and $h = 0.2$. The average Nusselt number improves when the Richardson number increases. It can be seen that, the Nu_{avg} increases with decreasing of the fin length where $Nu_{avg} = 7.31$, $Nu_{avg} = 8.14$ at $L_f = 0.6$, and $L_f = 0.2$, respectively.

Fig. 12. explains the influence of Reynold's number on the average Nusselt number (Nu_{avg}) a' the hot wall for $Pr = 7, Ri = 1$, and $L_f = 0.2$. The average Nusselt number enhances with a rising Reynold number due to increasing the influence of the force of inertia. Nu_{avg} increases when high the location of the fin (h) is, the increase at the maximum height of this fin

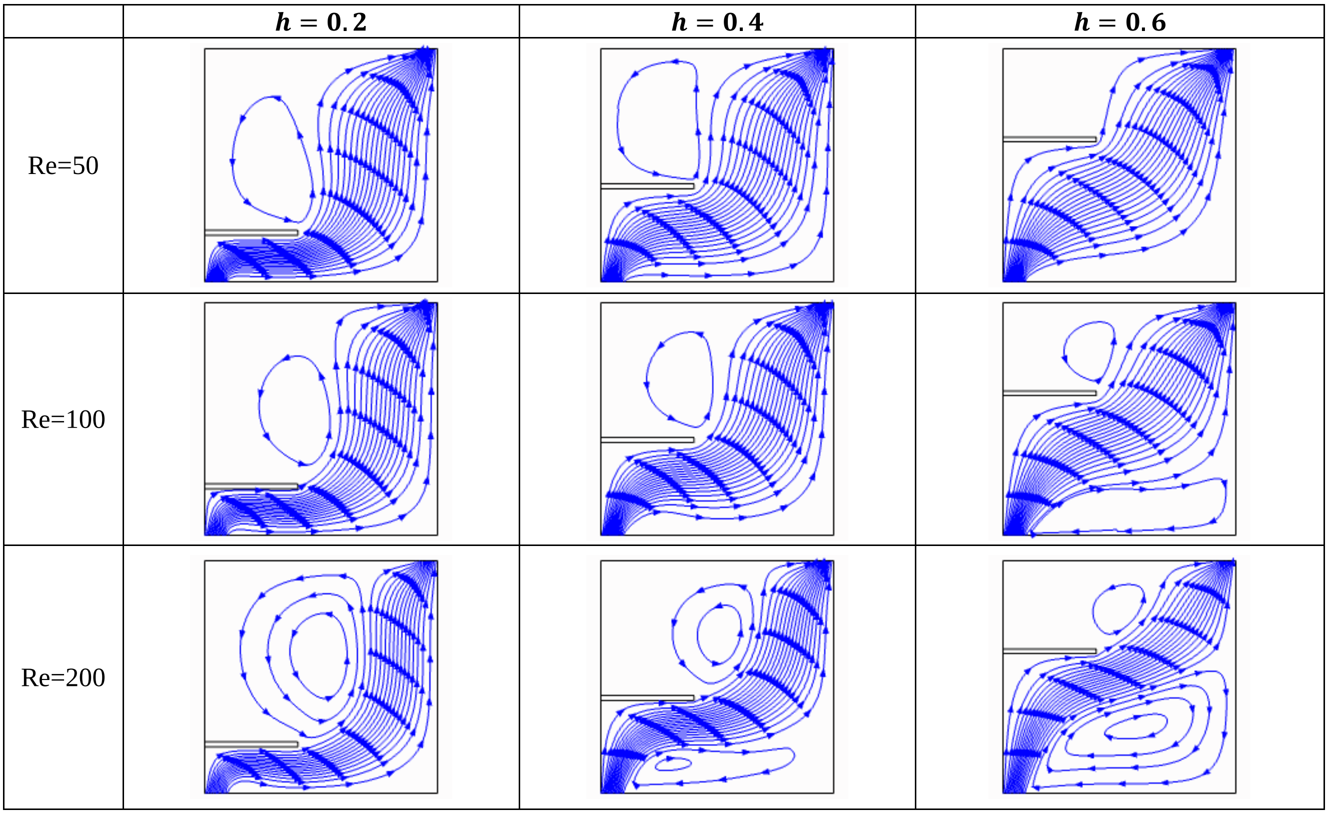

Figure 4. Streamlines for different Reynolds numbers and fin locations at $Pr = 7$, $Ri = 0.1$, $L_f = 0.4$.

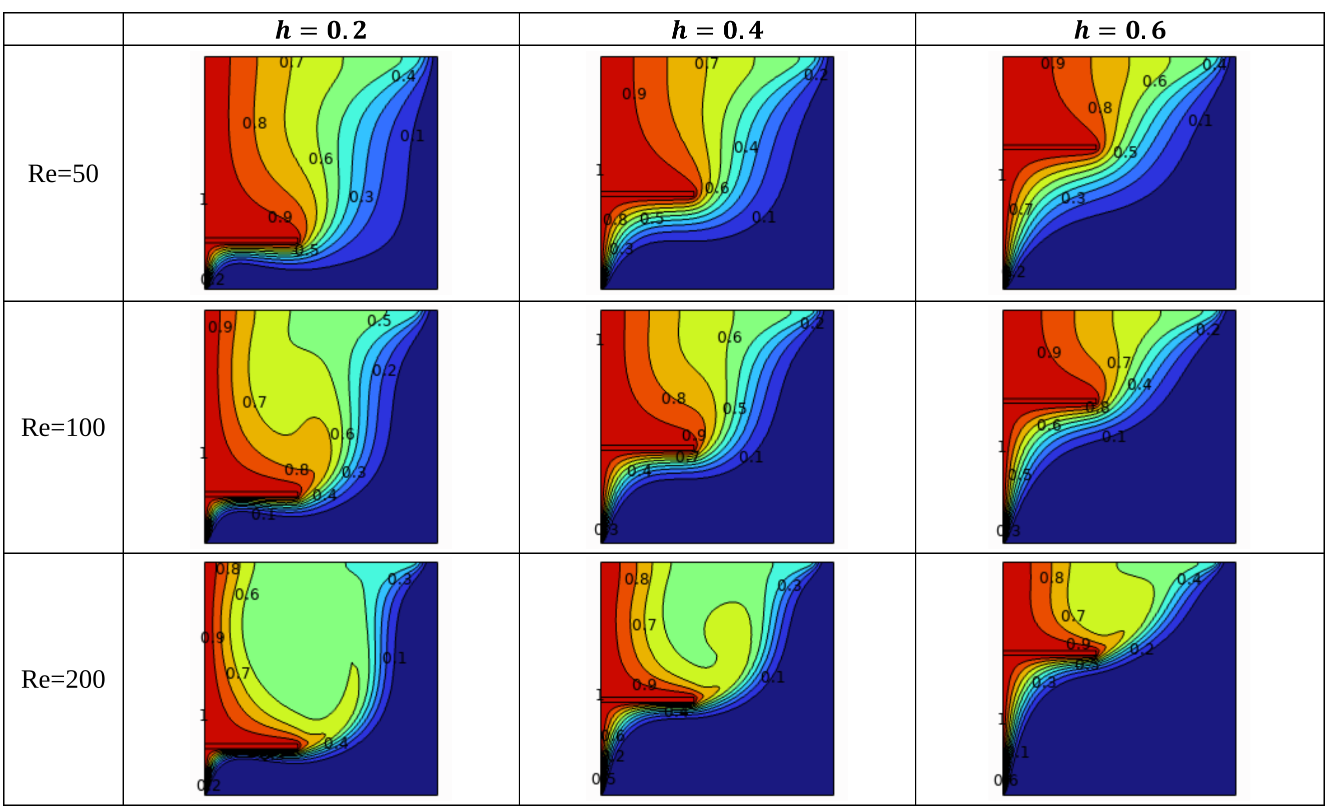

Figure 5. Isothermal for different Reynolds numbers and fin locations at $Pr = 7$, $Ri = 0.1$, $L_f = 0.4$.

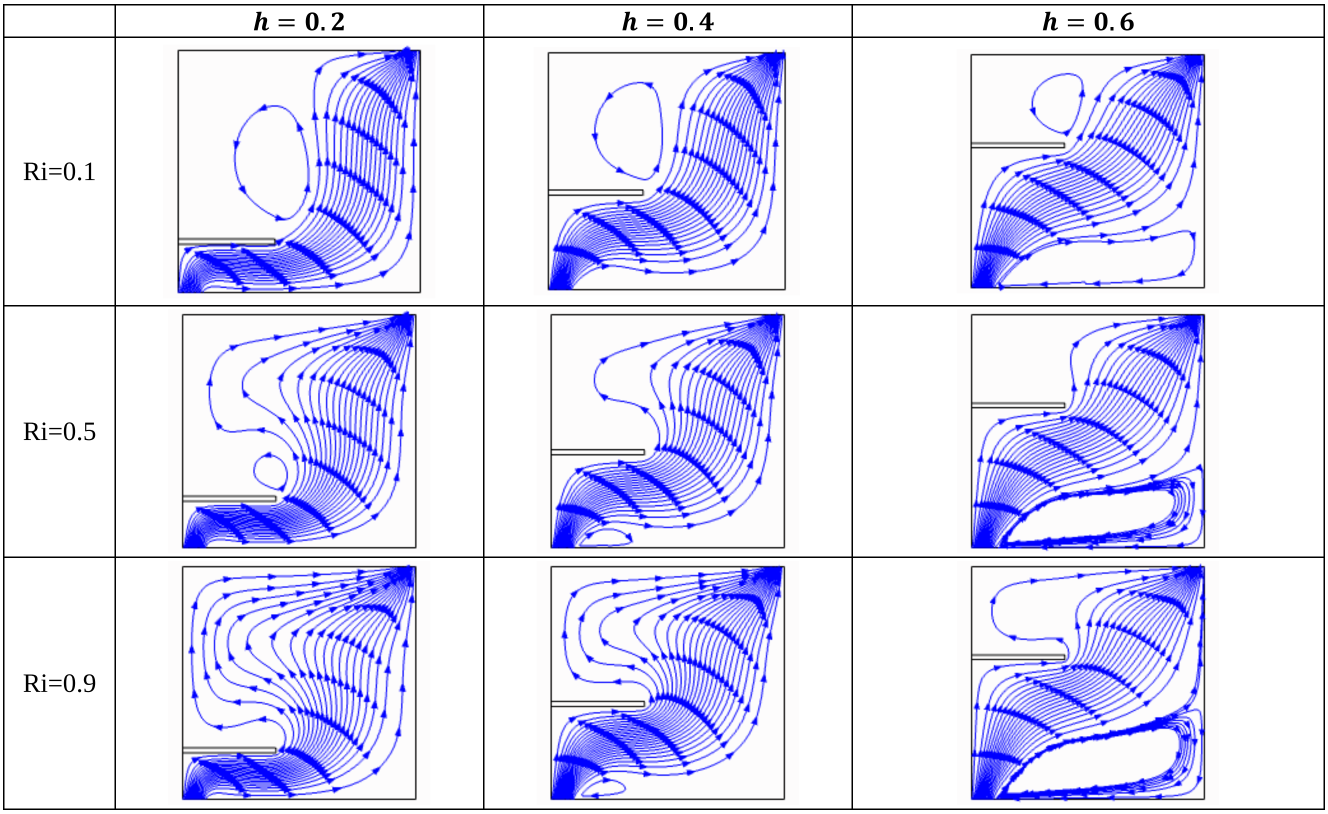

Figure 6. Streamlines for different Richards numbers and fin locations at $Pr = 7$, $Re = 100$, $L_f = 0.4$.

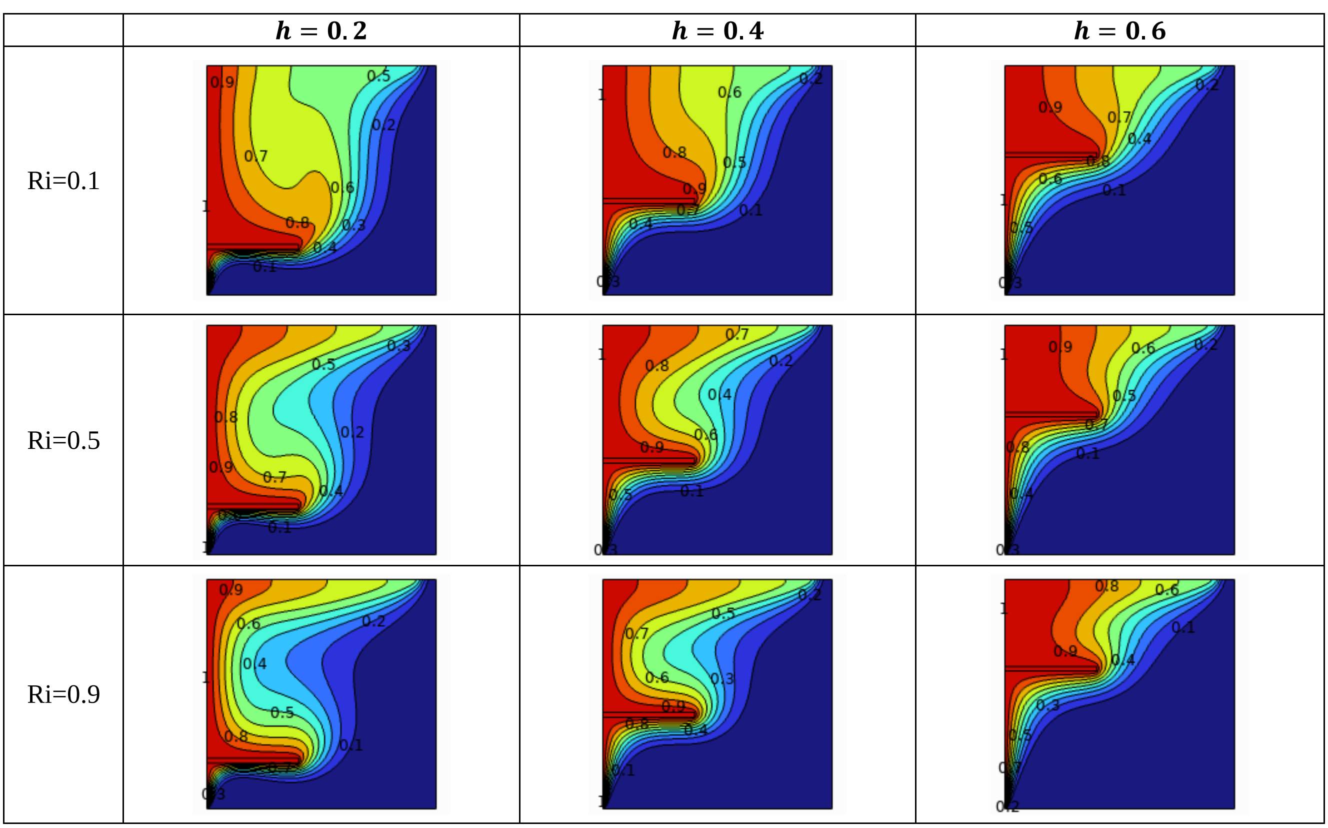

Figure 7. Isothermal for different Richards numbers and fin locations at $Pr = 7$, $Re = 100$, $L_f = 0.4$.

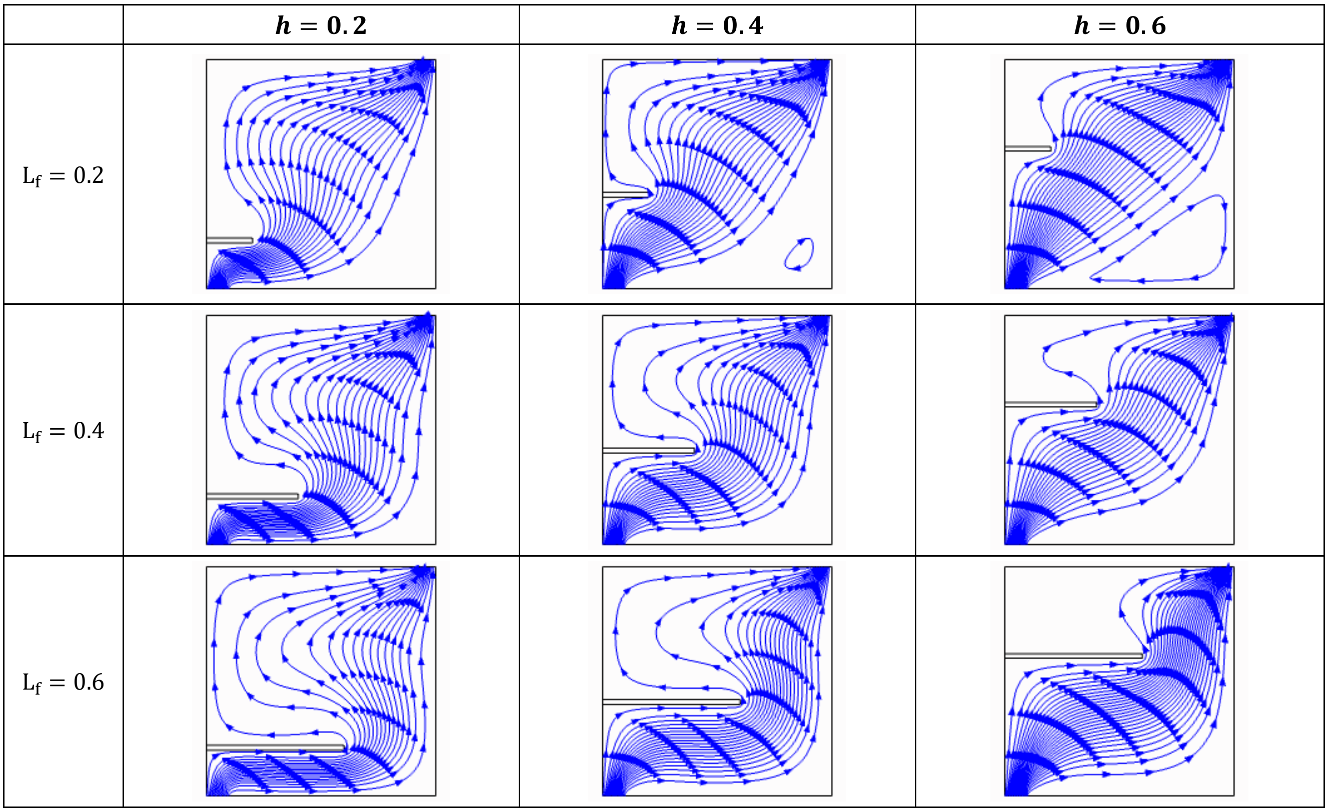

Figure 8. Streamlines for different fin lengths and fin locations at $Pr = 7$, $Re = 50$, $Ri = 1$.

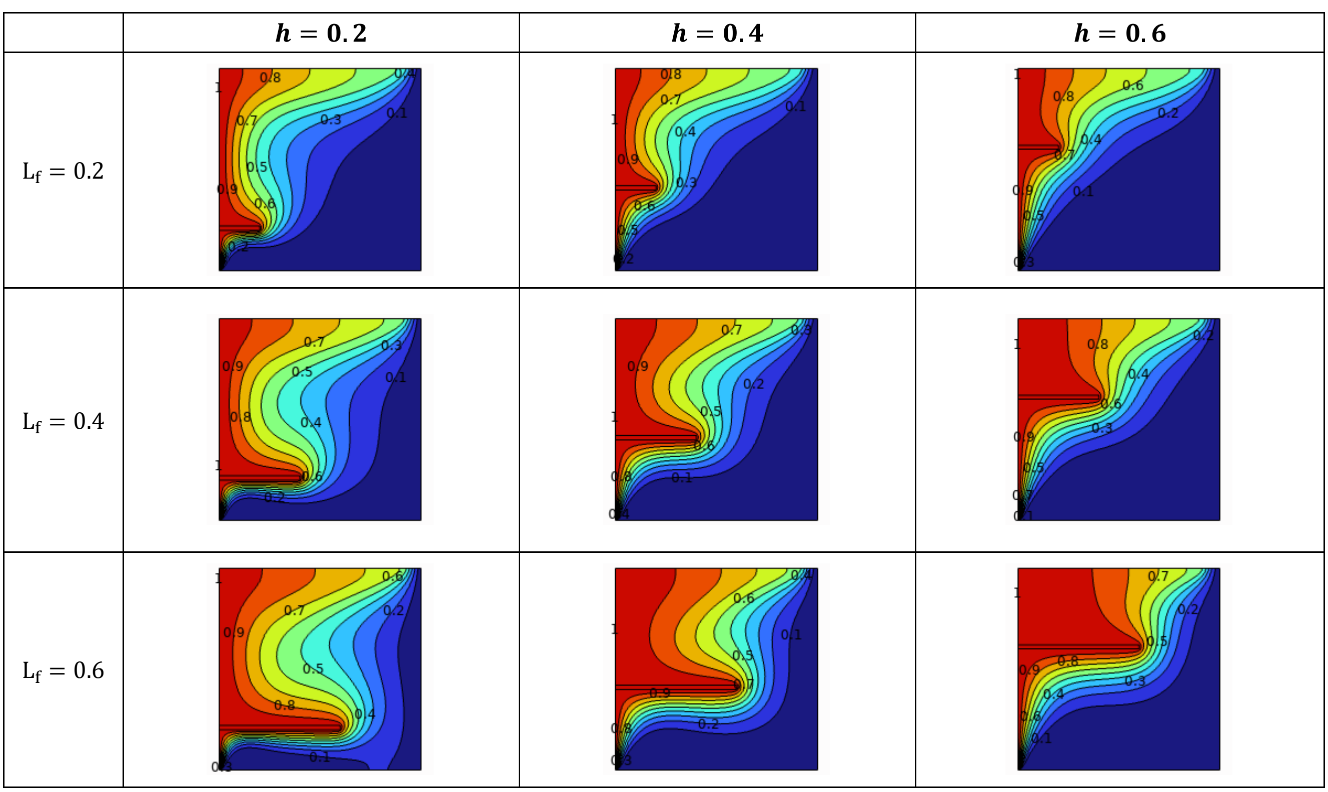

Figure 9. Isothermal for different fin lengths and fin locations at $Pr = 7$, $Re = 50$, $Ri = 1$.

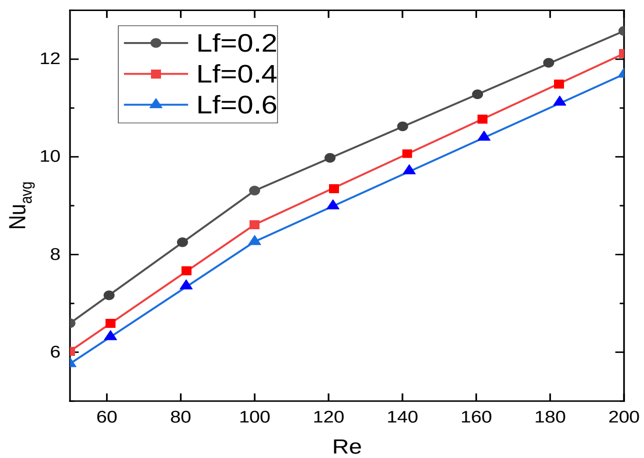

Figure 10. Average Nusselt number ($\boldsymbol{Nu_{avg}}$) on the left wall for various Re and fin lengths ($\boldsymbol{L_f}$) at $\boldsymbol{Pr=7, Ri=0.9, h=0.2}$.

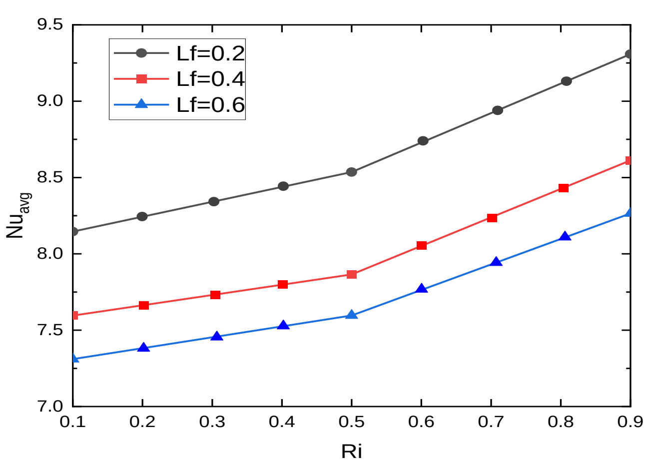

Figure 11. Average Nusselt number ($\boldsymbol{Nu_{avg}}$) on the left wall for various Ri and fin lengths ($\boldsymbol{L_f}$) at $\boldsymbol{Pr=7, Re=100, h=0.2}$.

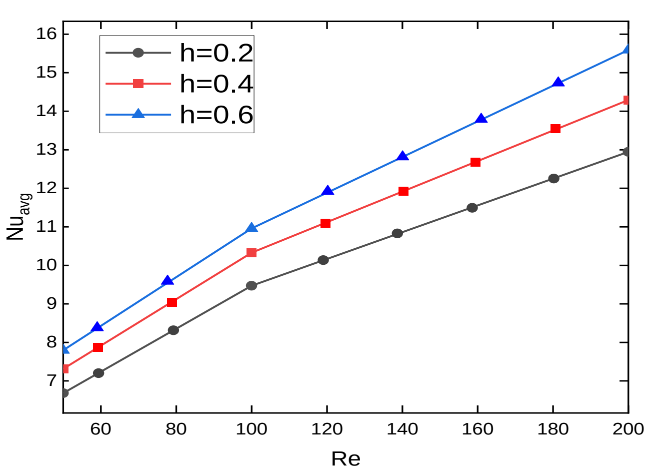

Figure 12. Average Nusselt number ($\boldsymbol{Nu_{avg}}$) on the left wall for various Re and fin locations ($\boldsymbol{h}$) at $\boldsymbol{Pr=7, Ri=1, L_f=0.2}$.

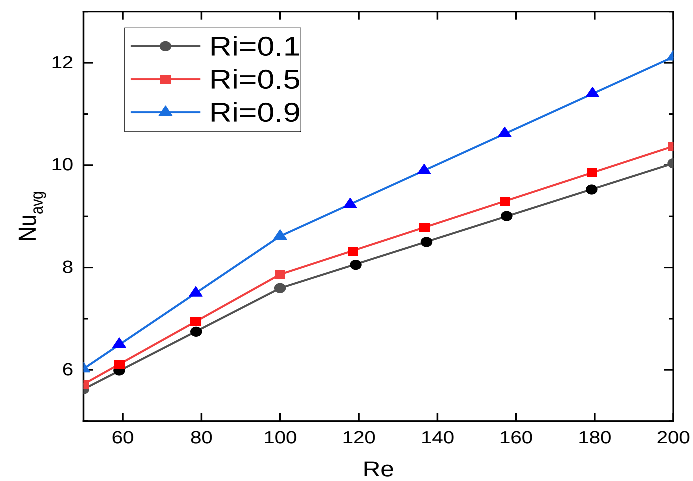

Figure 13. Average Nusselt number ($\boldsymbol{Nu_{avg}}$) on the left wall for various Re and Ri at $\boldsymbol{Pr=7, h=0.2, L_f=0.4}$.

location is estimated to be 17% due to an increase in the area of fluid flow on the hot wall caused by rising convective.

Fig. 13. explains the influence of Reynold's number and Richardson's number on the average Nusselt number (Nu_{avg}) at the hot wall for $Pr=7, h=0.2$, and $L_f=0.4$. When the Reynolds number increases, the average Nusselt number rises, indicating that the inertia force is expanding, where $Nu_{avg}=6.02$ at $Re=50$ and $Nu_{avg}=12.11$ at $Re=200$. It is also increasing as Richardson's number rises due to buoyancy force.

5. Conclusion

Laminar mixed convective in a vented square cavity with an existing fin is analyzed numerically in this paper. The fin is fixed on the hot vertical wall. The cold fluid enters the enclosure through the opening (W_{in}) in the lower left corner and escapes through the opening (W_{out}) in the upper right corner. Selection of the Prandtl number for fluid ($Pr=7$). The findings focus on the impact of Richardson's number (Ri), Reynold number (Re), fin lengths (L_f), and fin locations (h). The significant findings of this work are outlined:

1. Vortexes are very dense in the lower half of the container at a maximum fin location and high Richardson number due to the increased both buoyancy force influence and separation process.
2. The average Nusselt number increases with fin length decrease where $Nu_{avg}=7.31$ and 8.14 at $L_f=0.6$, and 0.2, respectively.
3. When the Reynold number rises from 50 to 200 for fin length ($L_f=0.6$), the average Nusselt number rises by approximately 50.68 % due to the influence of inertia forces.
4. Nu_{avg} increases when the height of the fin location (h) increases, at the maximum height of this fin location, $Nu_{avg}$is estimated to be 17% and that was due to an increase in the area of fluid flow on the hot wall caused by rising convective.

Authors' contribution

All authors contributed equally to the preparation of this article.

Declaration of competing interest

The authors declare no conflicts of interest.

Funding source

This study didn't receive any specific funds.

REFERENCES

[1] M.M. Rashidi, I. Mahariq, M. Alhuyi Nazari, O. Accouche, M.M. Bhatti, Comprehensive review on exergy analysis of shell and tube heat exchangers, Journal of Thermal Analysis and Calorimetry, 147(22) (2022) 12301-12311 DOI: https://doi.org/10.1007/s10973-022-11478-2.

[2] W. Liu, Y. Bie, T. Xu, A. Cichon, G. Królczyk, Z. Li, Heat transfer enhancement of latent heat thermal energy storage in solar heating system: A state-of-the-art review, Journal of Energy Storage, 46 (2022) 103727 DOI: https://doi.org/10.1016/j.est.2021.103727.

[3] G. Chen, Y. Tang, Z. Wan, G. Zhong, H. Tang, J. Zeng, Heat transfer characteristic of an ultra-thin flat plate heat pipe with surface-functional wicks for cooling electronics, International Communications in Heat and Mass Transfer, 100 (2019) 12-19 DOI: https://doi.org/10.1016/j.icheatmasstransfer.2018.10.011.

[4] B. Hiba, F. Redouane, W. Jamshed, C. Ahamed Saleel, S. Suriya Uma Devi, M. Prakash, K.S. Nisar, V. Vijayakumar, M.R. Eid, A novel case study of thermal and streamline analysis in a grooved enclosure filled with (Ag–MgO/Water) hybrid nanofluid: Galerkin FEM, Case Studies in Thermal Engineering, 28 (2021) 101372 DOI: https://doi.org/10.1016/j.csite.2021.101372.

[5] B. Al-Muhja, K. Al-Farhany, Numerical Investigation of the Effect of Baffle Inclination Angle on Nanofluid Natural Convection Heat Transfer in A Square Enclosure, Al-Qadisiyah Journal for Engineering Sciences, 12 (2019) 61-71 DOI: https://doi.org/10.30772/qjes.v12i2.589.

[6] K. Al-Farhany, B. Al-Muhja, L. Karuppusamy, U. Periyasamy, F. Ali, I. Sarris, Analysis of Convection Phenomenon in Enclosure Utilizing Nanofluids with Baffle Effects, Energies, 15 (2022) 6615 DOI: https://doi.org/10.3390/en15186615.

[7] K. Al-Farhany, B. Al-Muhja, F. Ali, U. Khan, A. Zaib, Z. Raizah, A.M. Galal, The Baffle Length Effects on the Natural Convection in Nanofluid-Filled Square Enclosure with Sinusoidal Temperature, in: Molecules, 2022.

[8] M. Almaliki, K. Al-Farhany, I. Sarris, Heat Transfer in an Inclined Rectangular Cavity Filled with Hybrid Nanofluid Attached to a Vertical Heated Wall Integrated with PCM: An Experimental Study, Symmetry, 14 (2022) 2181 DOI: https://doi.org/10.3390/sym14102181.

[9] K. Al-Farhany, M.F. Al-dawody, D.A. Hamzah, W. Al-Kouz, Z. Said, Numerical investigation of natural convection on Al2O3–water porous enclosure partially heated with two fins attached to its hot wall: under the MHD effects, Applied Nanoscience, (2021) DOI: https://doi.org/10.1007/s13204-021-01855-y.

[10] K. Al-Farhany, A. Abdulkadhim, H.K. Hamzah, F.H. Ali, A. Chamkha, MHD effects on natural convection in a U-shaped enclosure filled with nanofluid-saturated porous media with two baffles, Progress in Nuclear Energy, 145 (2022) 104136 DOI: https://doi.org/10.1016/j.pnucene.2022.104136.

[11] F. Selimefendigil, H. Öztop, Effects of an adiabatic inclined fin on the mixed convection heat transfer in a square cavity, Progress in Computational Fluid Dynamics, 14 (2014) 268-275 DOI: https://doi.org/10.1504/PCFD.2014.063864.

[12] S. Sivasankaran, K. Janagi, Numerical Study on Mixed Convection Flow and Energy Transfer in an Inclined Channel Cavity: Effect of Baffle Size, in: Mathematical and Computational Applications, 2022.

[13] R. Velkennedy, J. Jeseema Nisrin, K. Kalidasan, P. Rajeshkanna, Numerical investigation of convective heat transfer in a rectangular vented cavity with two outlets and cold partitions, International Communications in Heat and Mass Transfer, 129 (2021) 105659 DOI: https://doi.org/10.1016/j.icheatmasstransfer.2021.105659.

[14] Z.K. Radhi, Numerical study of mixed convection heat transfer through double square cavity connected with each other, Al-Qadisiya Journal For Engineering Sciences, 4 (2011).

[15] A. Abdulsahib, K. Al-Farhany, Experimental Investigation of Mixed Convection on a Rotating Circular Cylinder in a Cavity Filled With Nanofluid and Porous Media, Al-Qadisiyah Journal for Engineering Sciences, 13 (2020) 99-108 DOI: https://doi.org/10.30772/qjes.v13i2.653.

[16] F. Selimefendigil, A. Chamkha, MHD mixed convection of nanofluid in a three-dimensional vented cavity with surface corrugation and inner rotating cylinder, International Journal of Numerical Methods for Heat & Fluid Flow, 30 (2019) DOI: https://doi.org/10.1108/HFF-10-2018-0566.

[17] Z.A. Alhussain, Mixed convective flow in a multiple port ventilation square cavity with insulated baffle, Case Studies in Thermal Engineering, 30 (2022) 101785 DOI: https://doi.org/10.1016/j.csite.2022.101785.

[18] H. Shaker, M. Abbasalizadeh, S. Khalilarya, S.Y. Motlagh, Two-phase modeling of the effect of non-uniform magnetic field on mixed convection of magnetic nanofluid inside an open cavity, International Journal of Mechanical Sciences, 207 (2021) 106666 DOI: https://doi.org/10.1016/j.ijmecsci.2021.106666.

[19] L. Wang, W. Wang, C. Yang, D. Liu, F.-Y. Zhao, Mixed convection and heat flow characteristics in a lid-driven enclosure with porous fins: Full numerical modeling and parametric investigations, Numerical Heat Transfer, Part A: Applications, 77 (2019) 1-30 DOI: https://doi.org/10.1080/10407782.2019.1690351.

[20] M. Ali, R. Akhter, M.M. Alam, M. Miah, Magnetic-Mixed Convection in Nanofluid-Filled Cavity Containing Baffles and Rotating Hollow-Cylinders with Roughness Components, Mathematical Problems in Engineering, 2022 (2022) 1-25 DOI: https://doi.org/10.1155/2022/3044930.

[21] O. Çiçek, A.C. Baytaş, A numerical investigation of the particle behaviors and entropy generation in mixed convection inside a vented enclosure, International Journal of Thermal Sciences, 185 (2023) 108058 DOI: https://doi.org/10.1016/j.ijthermalsci.2022.108058.

[22] H.A. Dhahad, G.F. Al-Sumaily, W.H. Alawee, M.C. Thompson, Aiding and Opposing Re-circulating Mixed Convection Flows in a Square Vented Enclosure, Thermal Science and Engineering Progress, 19 (2020) 100577 DOI: https://doi.org/10.1016/j.tsep.2020.100577.

[23] M.A. Ismael, H.F. Jasim, Role of the fluid-structure interaction in mixed convection in a vented cavity, International Journal of Mechanical Sciences, 135 (2018) 190-202 DOI: https://doi.org/10.1016/j.ijmecsci.2017.11.001.

[24] H. Saleh, K. Naganthran, I. Hashim, M. Ghalambaz, R. Nazar, Role of fluid-structure interaction in free convection in square open cavity with double flexible oscillating fins, Alexandria Engineering Journal, 61(2) (2022) 1217-1234 DOI: https://doi.org/10.1016/j.aej.2021.04.073.

[25] M. Shahabadi, S.A.M. Mehryan, M. Ghalambaz, M. Ismael, Controlling the natural convection of a non-Newtonian fluid using a flexible fin, Applied Mathematical Modelling, 92 (2021) 669-686 DOI: https://doi.org/10.1016/j.apm.2020.11.029.

[26] M. Sathiyamoorthy, A. J. Chamkha, Analysis of natural convection in a square cavity with a thin partition for linearly heated side walls, International Journal of Numerical Methods for Heat & Fluid Flow, 24(5) (2014) 1057-1072 DOI: https://doi.org/10.1108/HFF-02-2012-0050.

[27] M. Rahman, M.A. Alim, S. Saha, M.K. Chowdhury, Mixed Convection in a Vented Square Cavity with a Heat Conducting Horizontal Solid Circular Cylinder, Journal of Naval Architecture and Marine Engineering, 5(2) (2009) 37-46 DOI: https://doi.org/10.3329/jname.v5i2.2504.